da allegare (in pdf) al PROOF dell'articolo:

Link sito dell'editore: https://www.sciencedirect.com/science/article/pii/S1359836818301021

Link codice DOI: https://doi.org/10.1016/j.compositesb.2018.03.045

Citazione bibliografica dell'articolo:

Nome autore, Cognome autore "Titolo articolo", pubblicato in nome rivista, anno, vol., fasc. pag.

P. Cavaliere, F. Jahantigh, A. Shabani, B. Sadeghi, "Influence of SiO2 nanoparticles on the microstructure and mechanical properties of Al matrix nanocomposites fabricated by spark plasma sintering", Composites Part B: Engineering Elsevier Science Publisher 146 (1) (2018) 60-68

Influence of SiO2 nanoparticles on the microstructure and mechanical properties of Al matrix nanocomposites fabricated by spark plasma sintering

Pasquale Cavaliere[a,*], Farhad Jahantigh[b], Ali Shabani[c], Behzad Sadeghi[d]

[a] Department of Innovation Engineering, University of Salento, Lecce, Italy
[b] Department of Photonics, Faculty of Physics, University of Kashan, Iran
[c] Young Researchers and Elite Club, Marvdasht Branch, Islamic Azad University, Marvdasht, Iran
[d] Young Researchers and Elite Club, Neyshabur Branch, Islamic Azad University, Khorasan Razavi, Islamic Republic of Iran

ARTICLE INFO

Keywords:
Spark plasma sintering
Al-SiO_2 nanocomposite
Mechanical properties
EBSD

ABSTRACT

Al-SiO_2 nanocomposite was produced using mechanical milling and spark plasma sintering (SPS) processes. In this research, the effects of ceramic nano size reinforcement on the microstructure and mechanical properties of the Al-SiO_2 nanocomposite were investigated. Using electron microscopy, the microstructures of the primary powder and the produced composites were studied. Microhardness and tensile tests were also employed to study the mechanical properties of the composites. The results revealed a reduction in porosity as increasing the nanoparticles percentage up to 3 wt%. For higher reinforcing percentages the material's density reached the minimum (86% of the density of the composite with 3 wt% of reinforcing particles). EBSD was employed to study the microstructural evolution of the produced materials.

1. Introduction

Particles-reinforced aluminum based composites are produced through various processing routes based on casting or powder metallurgy techniques. In general, powder metallurgy allows to obtain net-shape components starting from pre-alloyed particles applying pressure and heat in a controlled atmosphere [1–3]. Traditionally, ceramic particles and nanoparticles are introduced into the matrices via ingot casting, severe plastic deformation and powder metallurgy processes [4–6]. The conventional method of powder metallurgy (Ball milling and sintering) in normally employed to synthesize composites and nanocomposites, using relatively low cost and simple equipment [7,8]. Among the powder metallurgy technologies, spark plasma sintering represents the scientific and technological novelty able to obtain sound components with reduced porosity and enhanced mechanical properties. This method is becoming popular due to intrinsic advantages such as enhanced material properties, as well as lower processing temperature and shorter sintering time to consolidate powders compared to conventional methods [4,9,10]. SPS is conducted by applying pulsed high current and pressure in order to compact pre-mixed powders. The process is characterized by high heating rates (in the order of 1000 °C/min) and consequently reduced sintering times (in the order of few minutes). The heating power is not only distributed over the volume of the powder compact homogeneously in a macroscopic scale, but moreover the heating power is dissipated exactly at the locations in the microscopic scale, where energy is required for the sintering process, namely at the contact points of the powder particles [9,11,12]. Surface diffusion primarily allows the development of necking between particles, this is classified as a non-densifying mechanism of sintering. Avoiding this neck development maintains the small radius of curvature of pore-tips at higher temperatures. When processing temperatures reach the one sufficient for grain boundary diffusion, this small pore-tip radius drives higher diffusion rates, with consequent more rapid densification kinetics [13]. The reduced sintering time in SPS makes this technique very attractive also because of the reduced crystallite growth during heating [14]. Anyway, the starting powders microstructure results fundamental in retaining a very fine grain size [15–17].

Aluminum based metal matrix composites, due to their specific properties, are commonly used in aerospace, automotive and structural industries [5,18]. Recently, microstructure and mechanical properties of aluminum matrix composites and nanocomposites produced via SPS were investigated in the presence of different reinforcement particles and nanoparticles such as Al_2O_3 [12,19], SiC [6] and CNT [20–22].

The present study was aimed to evaluate the microstructure and mechanical properties of Al-SiO_2 nanocomposite fabricated by the SPS technique. For this purpose, Al-SiO_2 nanocomposites with 0, 3 and 6 wt

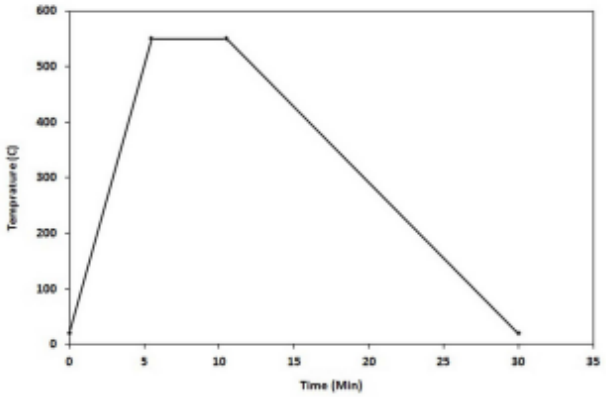

Fig. 1. Heating cycle diagram of the SPS process.

% of SiO_2 were produced with the aid of SPS process. Therefore, microstructure, hardness and tensile properties of the Al-SiO_2 nanocomposites with the various weight percent of SiO_2 nanoparticle were studied.

2. Experimental

The as-received aluminum powder (with average size < 20 μm) and nano size SiO_2 particles (with average size < 50 nm) were mixed by mechanical milling for 2 h. Nanocomposites containing 0, 3 and 6 wt.% of SiO_2 (Samples A1 to A3) were densified using SPS process. This process was carried out at a temperature of 550 °C and an applied vertical pressure of 50 MPa. A heating rate of 100 °C/min up to 550 °C was employed for the SPS followed by holding time of 5 min under the mentioned applied pressure. The cooling rate was 30 °C/min. The heating cycle diagram of the SPS process used in this study is shown in Fig. 1.

The phase composition was analyzed with an X-ray diffractometer (XRD). The microstructure of the produced nanocomposites was observed by a scanning electron microscope (SEM) equipped with an electron backscatter diffraction (EBSD) detector to investigate the effects of reinforcement content. Using Archimedes water immersion method, the relative density of the produced samples was calculated according to Eq. (1),

$$\rho = (w_d \rho w)/(w_d - w_w) \quad (1)$$

where ρ is the absolute density, w_d is dry weight, ρ_w is water density and w_w is the wet weight. In addition, the porosity of the produced samples was measured using Image J software processing the optical microscope (OM) micrographs.

The tensile test samples were machined from the SPSed composites. The gauge width and length of the tensile test samples were 2.5 and 6.4 mm, respectively (according to ASTM E8 for small size specimens). The room temperature tensile tests were performed with a Hounsfield H25KS testing machine. Vickers microhardness test were performed with a maximum load of 200 g and an indentation time of 15 s. Eight tests were performed per each sample.

3. Result and discussion

3.1. Microstructure

The XRD patterns of the sinter pure aluminum and Al-SiO_2 nanocomposites with different SiO_2 percentages are given in Fig. 2. The aluminum and SiO_2 phases are detected by XRD. It can be seen that, in the presence of SiO_2 nanoparticles, milling for 2 h could not change the position of aluminum peaks and they remained the same as those of

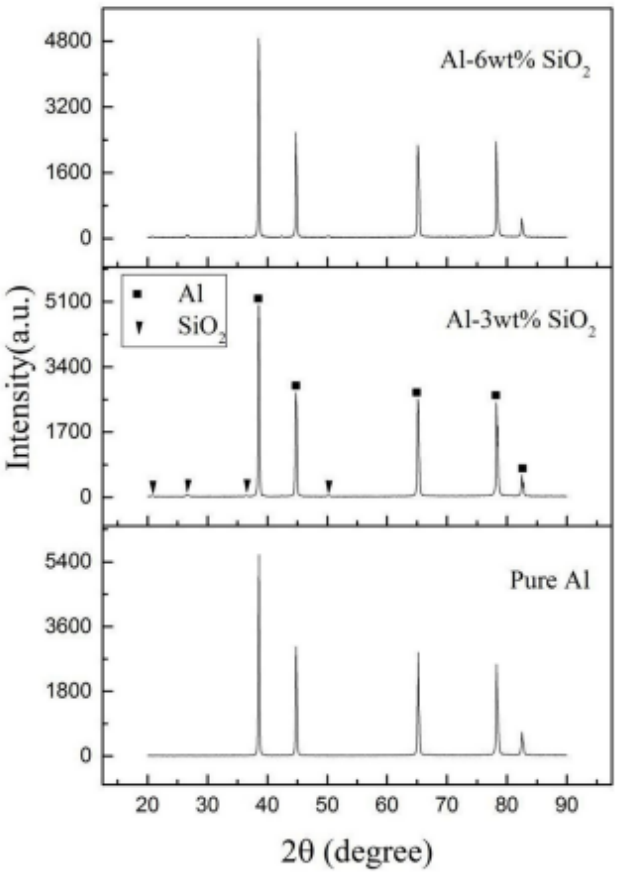

Fig. 2. XRD micrographs of the sintered pure aluminum and Al-SiO_2 nanocomposites.

pure aluminum. However, the intensity of the aluminum peaks decreased as a consequence of the addition of SiO_2 nanoparticles. It has been shown that there are some small peaks of SiO_2 in both the Al-SiO_2 nanocomposites. By increasing the SiO_2 nanoparticles content the effect of combined peak broadening and low intensity peaks of SiO_2 nanoparticles can be underlined. Besides, Razavi Hesabi and et al. [23] showed that when hard nanoparticles are added to the aluminum powder, the fracture occurs earlier. In other words, the presence of hard particles results in an increase in local fracture of the aluminum particles in the vicinity of the reinforcing particles. This could also enhance the work hardening rate of the matrix. Accordingly, all peaks' intensities decrease as increasing the SiO_2 nanoparticle content in the aluminum matrix.

Fig. 3a–c illustrate the microstructure of the employed primary powders. TEM micrograph of the SiO_2 nanoparticles is shown in Fig. 3a. In addition, SEM micrographs of the mixed powder of samples A2 and A3 are shown in Fig. 3b and c, respectively. The powders were ball milled for 2 h in order to have a uniformly mixed composite and also to break the agglomerated powders and consequently to obtain an homogeneous distribution of SiO_2 nanoparticles in the aluminum matrix.

The microstructures of the sintered Al-SiO_2 nanocomposites (A1 to A3) are also shown in Fig. 4a–f. As shown in Fig. 4a and b, the sample A1 has a uniform and completely sintered microstructure. It is shown in this figure that, by increasing the content of SiO_2 nanoparticles over 3 wt.% the pores link together and cause the formation of large pores in the aluminum matrix, especially in the vicinity of aluminum particles. However, for the 3 wt.% of SiO_2, a large number of open porosities were

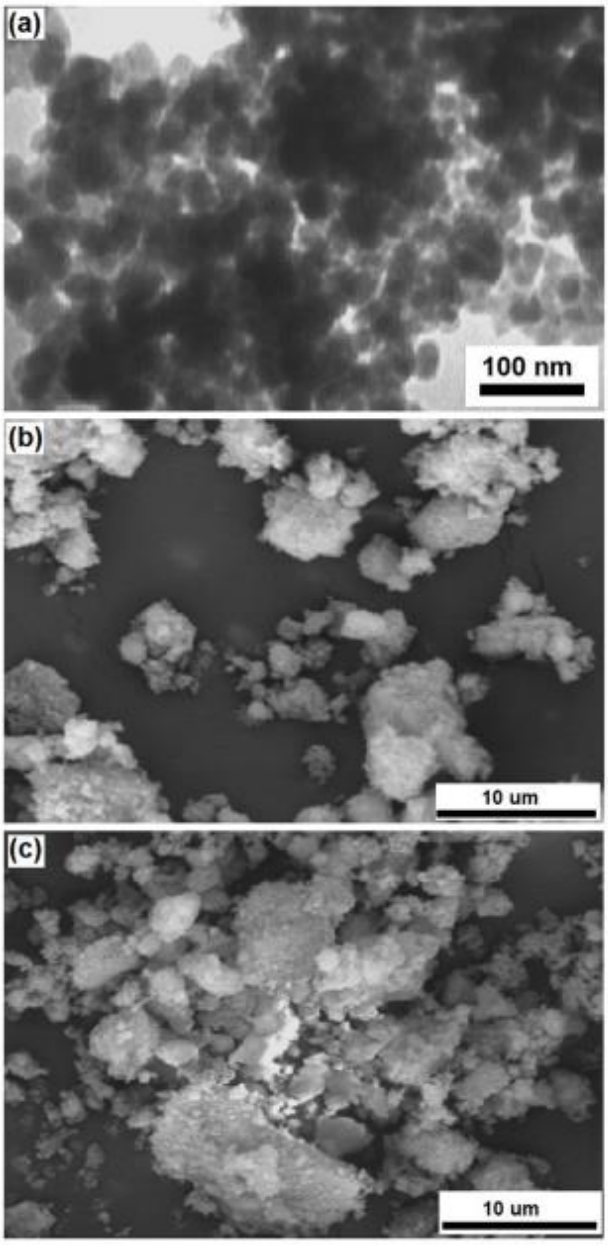

Fig. 3. a) TEM micrograph of the primary SiO_2 nanoparticles, b and c) microstructure of the ball milled composites A2 and A3 after 2 h milling, respectively.

filled by nanoparticles. In addition, it can be seen that aluminum particles grew quickly due to agglomeration of the SiO_2 nanoparticles. This causes the stagnation effect of grain boundaries pinning of aluminum through the presence of SiO_2 nanoparticle. This grain growth is observed to be more pronounced in the sample A3. These findings are consistent with those belonging to other researches [21,24,25]. In addition, Fig. 5 depicts the inverse pole figure maps of the sintered composites. The black color in the maps corresponds to the SiO_2 nanoparticles.

Fig. 5a shows the uniform grain size of the aluminum particles in the A1 sample revealing complete sintering in this sample. Fig. 5b and c also illustrate the abnormal grain growth and agglomeration of SiO2 nanoparticles; this phenomenon is amplified in the A3 sample. The maps in Fig. 5a–c shows an irregular assembly of large grains surrounded by relatively fine grains and some black zones, where no Kikuchi patterns could be recorded. This is usually the caseat grain boundaries, so grains with a size below the spatial resolution limit of EBSD are displayed in black. A bimodal grain size distribution was observed. In general, during the milling process for low times the material undergoes reduced deformation and the deformation energy is stored as plastic strain within the powders mixture. By applying high temperature in the Plasma Spark Sintering process, the stored energy can be released by recovery and recrystallization. When the primary recrystallization is complete, abnormal grain growth, in which single grains grow fast at the expense of smaller ones, can occur. A homogeneous dispersion of highly stable as well as high melting point oxide particles can retard such grain growth. Accordingly, this aspect can lead to remarkable variations in the mechanical properties and microstructure characteristics as shown in Fig. 5.

In Fig. 6, the pole figures (PF) are reported for the nano-composite with different SiO_2 weight percent. These figures show no texture or preferential grain orientation in the specimens. However, some texture components are shown in a {112} n110 m texture,4–6,11,21,22 corresponding to the {1-12} < 110 > and {-11-2} -1-10 > components of the ideal shear texture. These components indicate an amount of shear strain introduced into that material during the application of pressure during SPS processing. It is worth note that local overheating and a high density of necks due to a very fine initial powder would result in a faster dynamic recovery and recrystallization progress during sintering process. Consequently, high local temperatures are generated at the particle contacts causing abnormal grain growth. In this case, it is expected that no strong texture form in the SPSed samples. It should be emphasized that by increasing the SiO_2 weight percent {1-12} < 110 > and {-11-2} -1-10 > components change to the {1-11} -1-10 > as seen in Fig. 6.

The variation of porosity versus the amount of SiO_2 nanoparticles is shown in Fig. 7. It can be seen that the porosity decreased by increasing the amount of SiO_2 nanoparticles up to 3 wt.% and then it noticeably enhances by increasing amount of SiO_2 to 6 wt.%. By adding 3 and 6 wt.% of SiO_2 nanoparticle to the composite structure, porosity content decreased of 16% and then it increased of 280%, respectively. The density of the composite is directly affected by the porosity. Fig. 7 also reveals the variation of the density of the produced nanocomposites by increasing SiO_2 amount. It can be seen that by increasing SiO_2 nanoparticles to 3 and 6 wt.%, the density of the nanocomposites remains almost constant and then decreases noticeably by revealing a 14% of reduction. In other words, A2 and A3 have a theoretical density between 100 and 86% compared to the A1 sample. These results are consistent with the variation of the porosity of the composites. In fact, by increasing the porosity, the theoretical density of the composites decreases and, in turn, the reduction in theoretical density of the composite can strongly affect the mechanical properties of the composite. The main reasons for the increasing in porosity and reduction in the theoretical density by adding more than 3 wt.% of ceramic powder content are the following:

1. The agglomeration of the nanoparticles leads to a reduction of the densification of nanocomposites [8,12,26]. Nanoparticles have high specific surface and low compressibility [12], by enhancing the nanoparticles content, the theoretical density of the nanocomposite decreases. On the other hand, the agglomeration can cause enhancement in the interparticle distances of powders in the agglomerated regime.
2. Compressibility and formability of the ductile particles and hard particles in the nanocomposites decreased by enhancing the hard particle content [12,14,27]. This can be attributed to the increasing of the alumina-alumina contact which impedes the deformability of aluminum particles during compaction. Therefore, the lower compressibility of the particles leads to a decrease in the theoretical density.

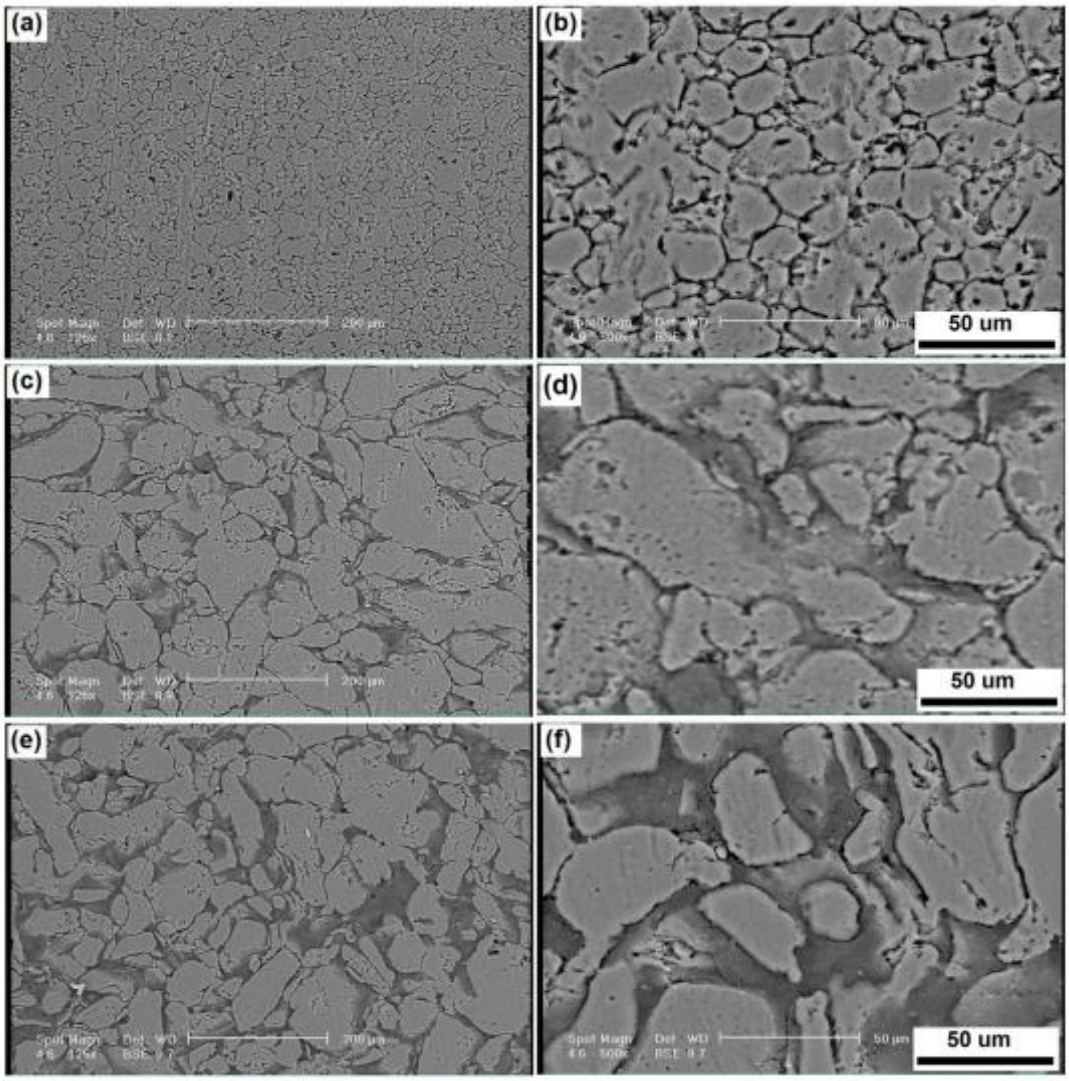

Fig. 4. SEM micrographs of the SPSed samples, a and b) A1, c and d) A2 and e and f) A3.

A common result, by adding reinforcing nanoparticles to the metallic matrix, is that mechanical properties are generally enhanced in comparison to the unreinforced matrix. This is mainly due to the increase in dislocation density [28]. In some cases, the presence of the ceramic powder between metallic particles or layers prevents strong diffusional bonding that results in the decrease of strength of nano and microcomposites. This can be intensified when the nanoparticles content exceeds 3 wt.%, the mechanical properties like strength, do not vary due to agglomeration of the nanoparticles within matrix microstructure [2]. In this situation, the bonding reduction of the powder particles in the nanocomposite leads to decreasing of the theoretical density, and consequently enhances the porosities content into microstructure. Figs. 4 and 5 depict the appropriate bonding between the aluminum particles in the A1 sample. In this sample aluminum particles first close together, stick, neck and bond due to induced pressure. The aluminum particles are quite large in size if compared to the SiO_2 particles, so they crates extra spaces for the accommodation of nanoparticles. By applying pressure and temperature at the same time, necking takes place between particles due to the different curvature of alumina and aluminum particles. It can be explained by stimulating of diffusional mechanisms like grain boundary and volume diffusion. Formation of bonding between particles during SPS process leads to a decrease in porosity content and consequently enhancement in the theoretical density. While, in the presence of the nanoparticles with further content 3-4 wt.% (Figs. 4f and 5c), the absence of the bonding between aluminum particles leads to the formation of the porosity and to the reduction of the theoretical density.

3.2. Mechanical properties

The mechanical properties of the nanocomposites were evaluated through tensile tests. The engineering stress–strain curves are presented in Fig. 8. The highest tensile strengths are recorded in pure Al (62 MPa) and Al-3wt. % SiO_2 (78 MPa) while Al-6wt. % SiO_2 revealed the lowest value. The pressure applied during the SPS is usually between 30 and 150 MPa. However, due to the decrease in the cross section at the particle-particle contact points, the local pressure raises up to 10000 MPa. Such a high local pressure besides high local temperature causes the breaking of the oxide layers on the aluminium particles surfaces resulting in direct metal to metal contacts. In this situation, mass transport mechanisms like grain boundary, volume and power law creep contribute to the neck formation. Therefore, considering local temperature and pressure at the SPS process, necking takes place easily between aluminium particles in the presence of SiO_2 nanoparticles.

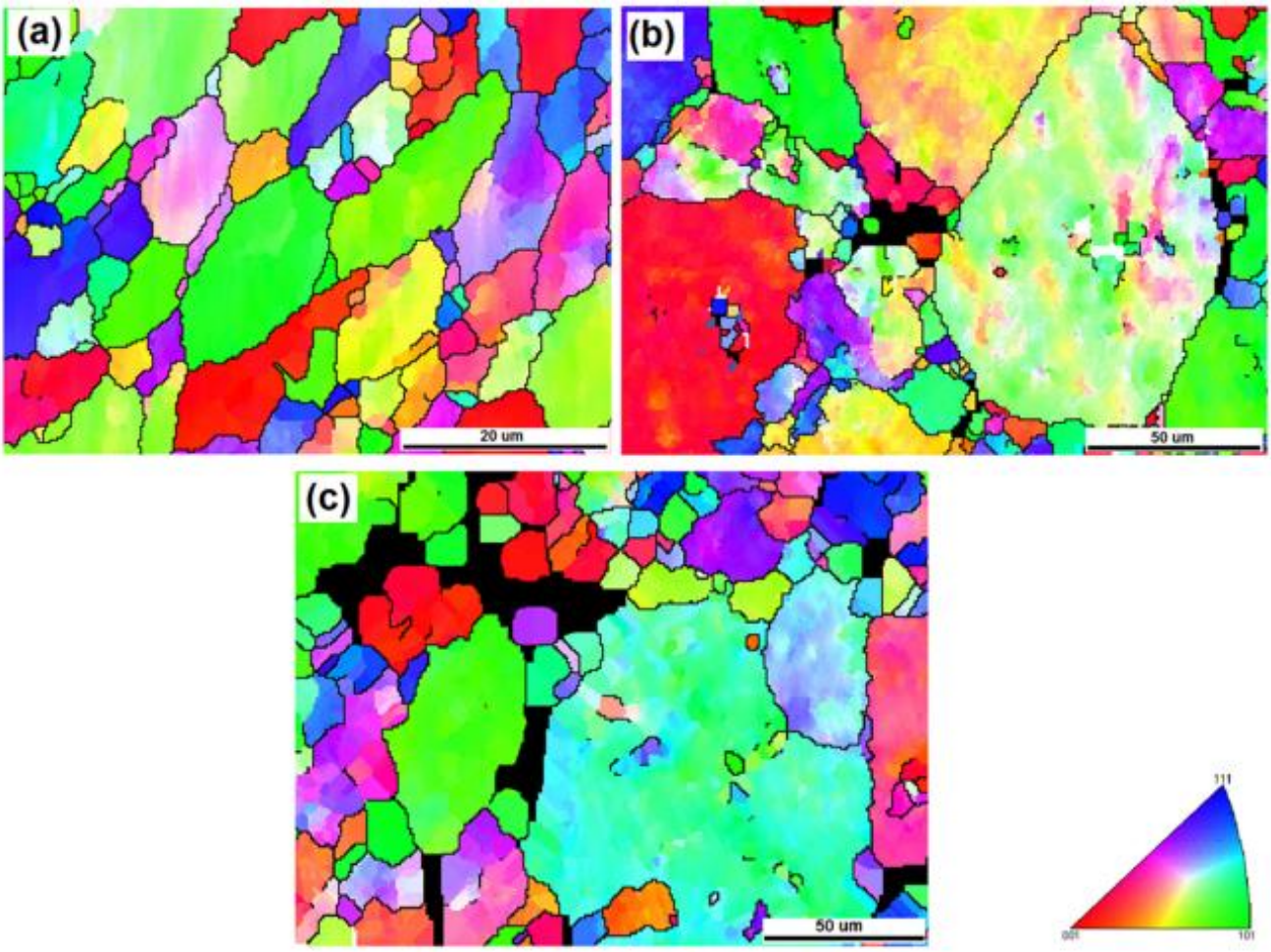

Fig. 5. Inverse pole figure maps of the SPSed samples, a) A1, b) A2 and c) A3.

Finally, it leads to high density value in the Al-3wt.% SiO_2 nanocomposite.

By increasing the content of the reinforcing phase, the SiO_2 nanoparticles are distributed typically along the grain boundaries of aluminum particles. Subsequently, a continuous brittle phase of SiO_2 nanoparticles forms along the grain boundaries. This causes an enhancement in the agglomeration of the SiO_2 nanoparticles leading to a decrease in the density value and consequently in the mechanical properties. Additionally, agglomeration of nanoparticles causes the increase of the interparticle distances leading to the strength decrease, based on the Orowan effect mechanism [29].

It can be seen that, by increasing ceramic nanoparticles in the composite structure more than 3 wt%, tensile properties strongly decrease. Fig. 9 reveals the tensile strength and elongation of the nanocomposite as a function of the nano-SiO_2 particles percentage. The tensile strength of the nanocomposite increased and then decreased in A2 and A3 samples, respectively. In addition, the elongation of the nanocomposites decreased with the SiO_2 nanoparticles amount. As shown in this figure, firstly the tensile strength increases from 62 to 78 and then decreases to 29 MPa for 6 wt.% of SiO_2 nanoparticles. These variations in tensile strength illustrate 26% increase and 60% reduction in strength of the nanocomposite, respectively. Furthermore, according to this figure, elongation of the nanocomposite revealed 9% and 50% reduction by addition of 3 wt.% and 6 wt.% of SiO_2 nanoparticles, respectively. Generally, the presence of ceramic particles and nanoparticles, for content lower than 3 wt.%, in the sintered composites, leads to the improvement of the mechanical properties [2,12,30]. Nevertheless, the following factors govern this variation of mechanical properties of the mentioned nanocomposites:

1. Reinforcement amount. As mentioned above, compressibility and formability of the ductile and hard particles in the nanocomposites decrease by enhancing the hard particle content [12,14,27]. Therefore, for a content of nanoparticles higher than 3 wt.%, incompressibility of the strain hardened nanocomposites promoted the formation of micro-voids along the boundaries and at the triple points [31]. The formation of micro-voids leads to the reduction in tensile strength and elongation. In addition, in the A2 sample, cracks propagate reaching the SiO_2 nanoparticles, distributed at the boundaries of the aluminum grains. Therefore, it is difficult for the crack to cross the SiO_2 particles and the crack is deflected propagating along the aluminum and SiO_2 grains boundaries. Consequently, the strength increases due to this phenomenon. On the other hand, by increasing SiO_2 nanoparticles amount, due to enhancement of the porosity and the particle distance, crack propagation increases in the A3 sample and reduces the strength, remarkably.
2. Porosity. As far as, the content of the SiO_2 nanoparticles is lower than 3 wt.%, a large number of open porosities are filled by nanoparticles and it causes an enhancement in the density. On the other hand, for further amount of SiO_2 nanoparticles (more than 3 wt.% in this study) the porosity content between the aluminum particles and

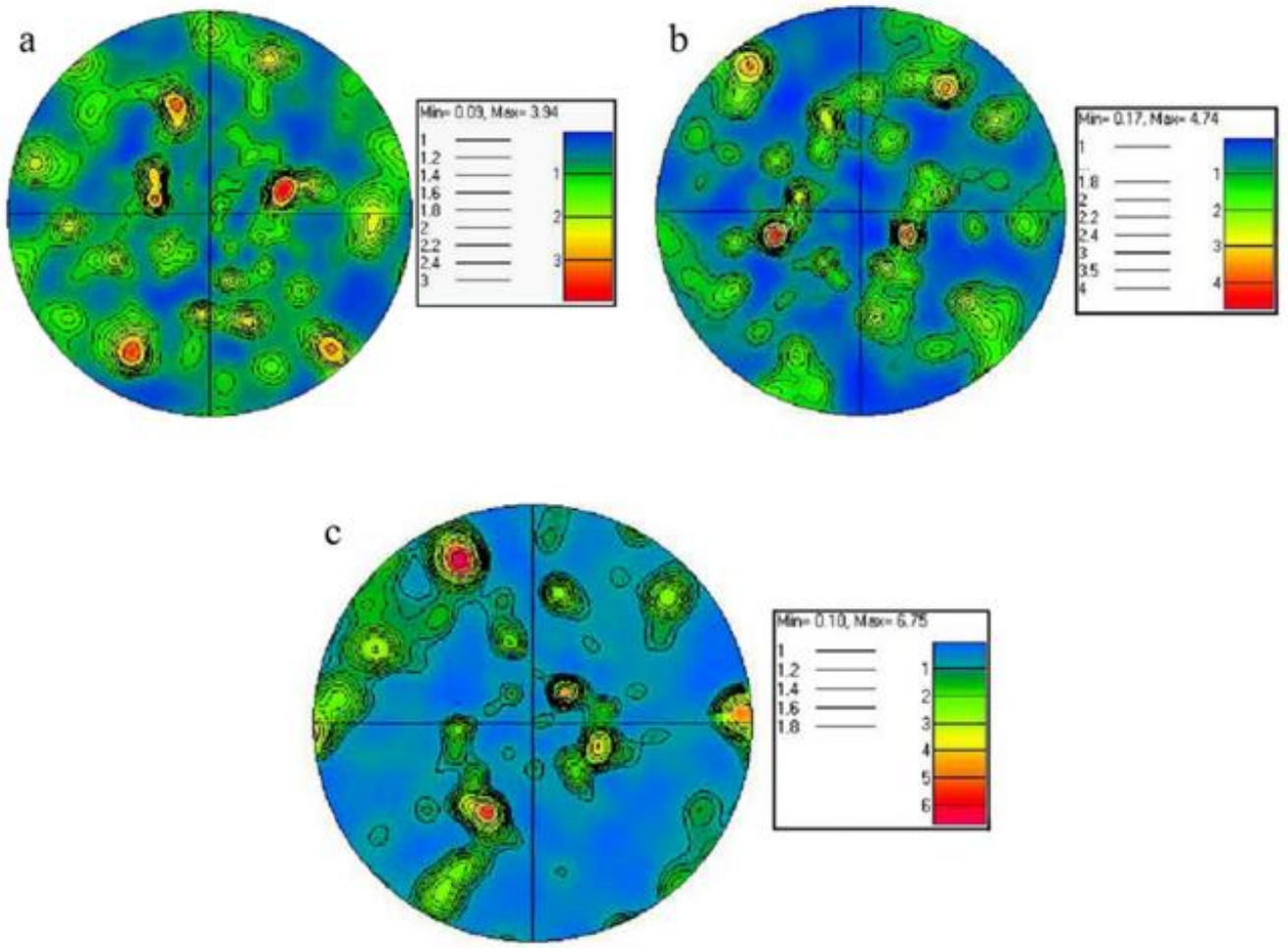

Fig. 6. Pole figure of the SPSed samples, a) A1, b) A2, c) A3.

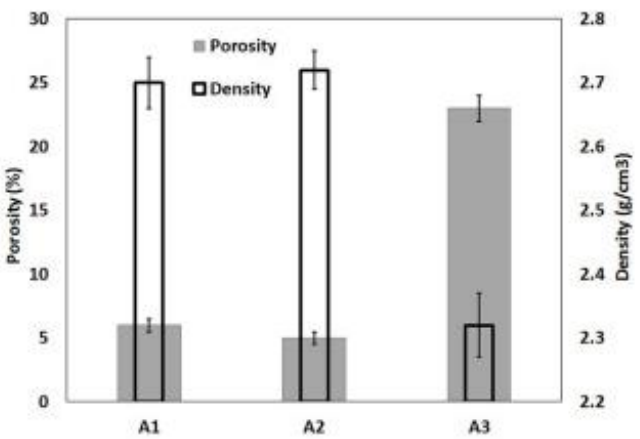

Fig. 7. Variation of the porosity and theoretical density of the produced nanocomposites A1 to A3 versus the amount of SiO_2 nanoparticle.

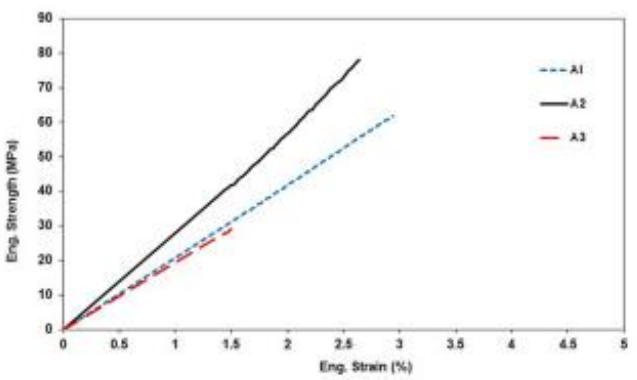

Fig. 8. Engineering stress–strain curves of the produced nanocomposites.

the SiO_2 nanoparticles increases, this is one of the crucial factors for the reduction of the material density. During tensile test, these pores notably reduce the tensile properties of the composites. The agglomeration of nanoparticles can also increase the interparticle distances, subsequently decreasing the energy required for the dislocation motion when they encounter a SiO_2 nanoparticle (Eq. (2) [32]).

$$\tau_0 = Gb/l \quad (2)$$

$\tau_\bigcirc$ is the stress required for a dislocation motion to pass reinforcement, G is the shear modulus of the matrix and b is the burger vector of the dislocation.

3. Grain size. During the SPS process, aluminum particles grow due to

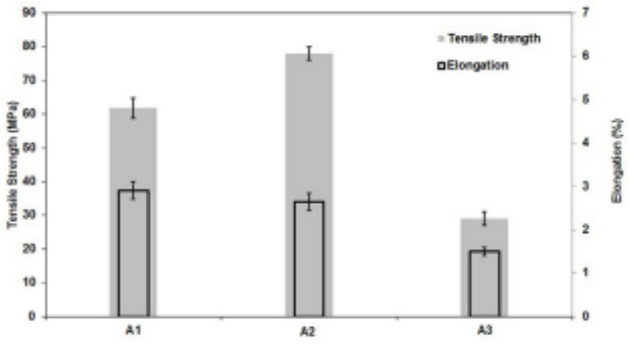

Fig. 9. Variation of the tensile strength and the elongation of the produced nanocomposites versus the amount of the SiO_2.

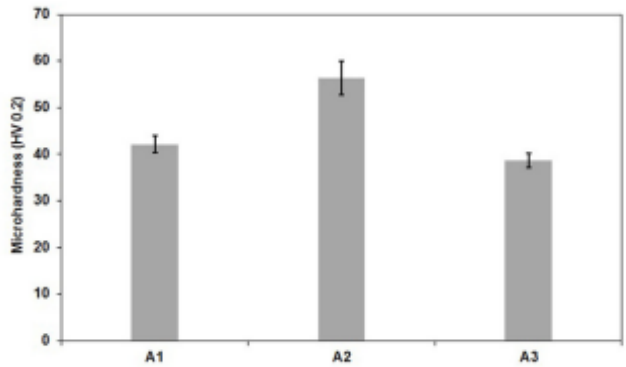

Fig. 11. Variation of the microhardness versus SiO_2 nanoparticle amount.

agglomeration of SiO_2 nanoparticles which result in the formation of porosity around them. Generally, grain growth leads to a decrease in tensile strength of the composites [12,33]. Fig. 10 shows the grain size distribution histograms of the A1 to A3 sample obtained via EBSD. Fig. 10 indicates that the grain size distribution showed little change after adding 3 and 6 wt.% of SiO_2 nanoparticles. It can be seen that the grain size increases by enhancing the SiO_2 nanoparticles percentage however, grain size distribution is more uniform in the A2 sample comparing to A3.

4. Bonding quality. Bonding quality between particles is reduced in the presence of nanoparticles [12,33]. Absence of the bonding between aluminum particles leads to the formation of micro-voids and cracks during tensile test. Tensile strength and elongation of the composites decrease notably due to formation of micro-voids and cracks.

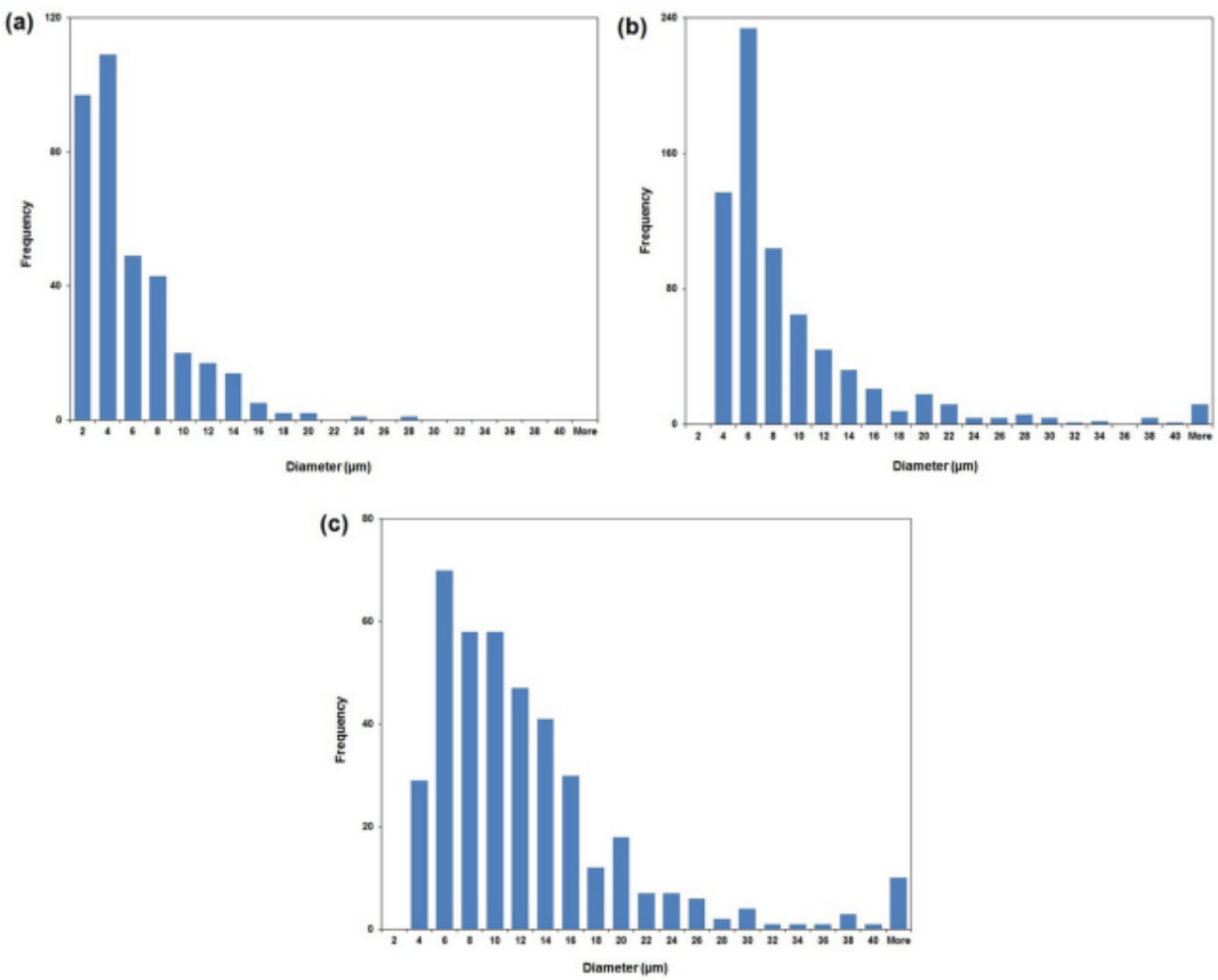

Fig. 10. Grain size distribution histograms of the SPSed samples, a) A1, b) A2 and c) A3.

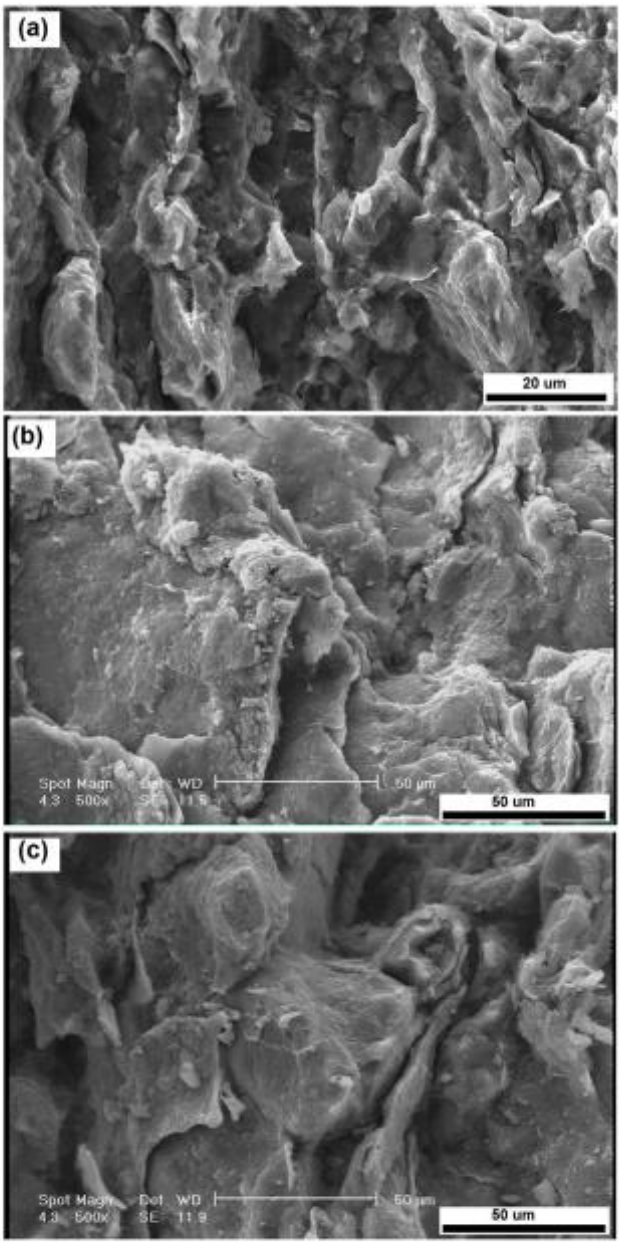

Fig. 12. SEM fractographs of the A1 to A3 samples.

The microhardness variation of the nanocomposites with SiO_2 amount is illustrated in Fig. 11. An increase of about 34% (from 42 to 56) in the microhardness was seen by adding 3 wt.% of SiO_2 nanoparticles to the composite. It can be attributed to homogeneous dispersion of the SiO_2 nanoparticles in the aluminum matrix. The microhardness value first increases to approximately 56 HV for the sample containing 3 wt.% of nanoparticles, and then it decreases to 39 HV for higher content of nanoparticles. It can be explained that for low content of nanoparticles, the uniform dispersion of the SiO_2 nanoparticles in aluminum matrix takes place with consequent lower interparticle distances between aluminum powder particles. This can increase the required energy for plastic deformation and accordingly increases the microhardness. However, the increase of the microhardness of the A2 sample is considerable while the A3 sample revealed about 8% decrease in the microhardness, comparing to A1 sample. This weakening in the microhardness for SiO2 content higher than 3 wt.% is governed by the factors explained above, such as increasing in the reinforcement amount, enhancement of the porosity, grain growth and decreasing of the bonding quality of the particles.

Fig. 12 reveals the fractographs of the studied materials samples after tensile test. Grain growth in the A2 and A3 sample is clearly revealed by the fracture surfaces. Better quality of bonding between Al particles in A1 and A2 samples comparing with A3 are also shown by these pictures. Brittle and intergranular modes of fracture in all the samples can be seen in Fig. 12. Generally, intergranular fracture, smooth surface without formation of dimples, low amount of plastic deformation and cleavage facets and striations are characteristic features of brittle fracture. As can be seen in these figures, intergranular fracture without formation of dimples occurs in the samples, presenting a brittle fracture in all the samples.

4. Conclusion

By spark plasma sintering, Al-SiO_2 nanocomposites were produced at a temperature of 550 °C and an applied vertical pressure of 50 MPa. The effect of adding SiO_2 nanoparticles on the microstructure and mechanical properties of the composites has been investigated. The results revealed that by increasing the SiO_2 nanoparticle amount more than 3 wt.% leads to agglomeration of particles, grain growth of aluminum, enhancement in the porosity and reduction in the theoretical density of the composite. By increasing the SiO2 weight percent {1-12} < 110 > and {-11-2} -1-10 > components change to the {1-11} -1-10 > . Tensile strength of the nanocomposite increased more than 25% by addition of 3 wt.% SiO_2 nanoparticle. However, tensile properties of the composite remarkably weakened due to decreasing in the microstructure quality of the produced composites for further amount of SiO_2 nanoparticle. It was found that by increasing the SiO_2 nanoparticles content, the microhardness values of the nanocomposite first increases and then decreases when the amount of the nanoparticles exceeds 3 wt %. In addition, brittle and intergranular mode of fracture was seen in the samples.

Appendix A. Supplementary data

Supplementary data related to this article can be found at http://dx.doi.org/10.1016/j.compositesb.2018.03.045.

References

[1] Zhang Z, Chen D. Contribution of Orowan strengthening effect in particulate-reinforced metal matrix nanocomposites. Mater Sci Eng 2008;A483:148–52.
[2] Kang Y-C, Chan SL-I. Tensile properties of nanometric Al2O3 particulate reinforced aluminium matrix composites. Mater Chem Phys 2004;85:438–43.
[3] Shabani A, Toroghinejad MR. Investigation of the microstructure and the mechanical properties of Cu-NiC composite produced by accumulative roll bonding and coating processes. J Mater Eng Perform 2015;24:4746–54.
[4] Tjong SC, Ma Z. Microstructural and mechanical characteristics of in situ metal matrix composites. Mater Sci Eng 2000;R29:49–113.
[5] Shabani A, Toroghinejad MR, Shafyei A. Fabrication of Al/Ni/Cu composite by accumulative roll bonding and electroplating processes and investigation of its microstructure and mechanical properties. Mater Sci Eng 2012;A558:386–93.
[6] Mizuuchi K, Inoue K, Agari Y, Nagaoka T, Sugioka M, Tanaka M, Takeuchi T, Tani J-I, Kawahara M, Makino Y. Processing of Al/SiC composites in continuous solid–liquid co-existent state by SPS and their thermal properties. Composites Part B 2012;43:2012–9.
[7] Suryanarayana C. Mechanical alloying and milling. Prog Mater Sci 2001;46:1–184.
[8] Roy D, Sinha A, Chattopadhyay P, Manna I. Nanoindentation behavior of bulk metastable Al 65 Cu 20 Ti 15 alloy prepared by consolidation of the ball milled powder. Mater Sci Eng 2011;A528:8047–50.
[9] Wang H, Jin Z, Miyamoto Y. Ti3SiC2/Al2O3 composites prepared by SPS. Ceram Int 2003;29:539–42.
[10] Ge W, Wang Y, Shang C, Zhang Z, Wang YJ. Mater Sci 2017;52:5726-37.
[11] Tokita M. Trends in advanced SPS spark plasma sintering systems and technology. J Soc Powd Tech 1993;30:790–804.
[12] Dash K, Chaira D, Ray BC. Synthesis and characterization of aluminium–alumina micro- and nano-composites by spark plasma sintering. Mater Res Bull 2013;48:2535–42.
[13] Olevsky EA, Froyen L. Impact of thermal diffusion on densification during SPS. J

Am Ceram Soc 2009;92:S122–32.
[14] Saheb N, Aliyu IK, Hassan SF, Al-Aqeeli N. Matrix structure evolution and nanoreinforcement distribution in mechanically milled and spark plasma sintered Al-SiC nanocomposites. Materials 2014;7:6748–67.
[15] Kubota M, Wynne PB. Electron backscattering diffraction analysis of mechanically milled and spark plasma sintered pure aluminium. Scripta Mater 2007;57:719–22.
[16] Vintila R, Charest A, Drew RAL, Brochu M. Synthesis and consolidation via spark plasma sintering of nanostructured Al-5356/B4C composite. Mater Sci Eng 2011;A528:4395–407.
[17] Bathul S, Anandani RC, Dhar A, Srivastava AK. Microstructural features and mechanical properties of Al 5083/SiCp metal matrix nanocomposites produced by high energy ball milling and spark plasma sintering. Mater Sci Eng 2012;A545:97–102.
[18] Shabani A, Toroghinejad MR, Shafyei A. Compressive, shear, and fracture behavior of CNT reinforced Al matrix composites manufactured by severe plastic deformation. Mater Des 2012;40:212–20.
[19] Razavi-Tousi S, Yazdani-Rad R, Manafi S. Effect of volume fraction and particle size of alumina reinforcement on compaction and densification behavior of Al–Al 2 O 3 nanocomposites. Mater Sci Eng 2011;A521:1105–10.
[20] Kwon H, Estili M, Takagi K, Miyazaki T, Kawasaki A. Combination of hot extrusion and spark plasma sintering for producing carbon nanotube reinforced aluminum matrix composites. Carbon 2009;47:570–7.
[21] Cavaliere P, Sadeghi B, Shabani A. Carbon nanotube reinforced aluminum matrix composites produced by spark plasma sintering. J Mater Sci 2017;52:8618–29.
[22] Krommenhoek M, Shamma M, Morsi K. Processing, characterization, and properties of aluminum–carbon nanotube open-cell foams. J Mater Sci 2017;52:3927–35.
[23] Hesabi ZR, Simchi A, Reihani SS. Structural evolution during mechanical milling of nanometric and micrometric Al2O3 reinforced Al matrix composites. Mater Sci Eng 2006;A428:159–68.
[24] Sadeghi B, Shamanian M, Ashrafizadeh F, Cavaliere P, Rizzo A. Influence of Al2O3 nanoparticles on microstructure and strengthening mechanism of Al-Based nanocomposites produced via spark plasma sintering. J Mater Eng Perform 2017;26:2928–36.
[25] Liu H-W, Bishop DP, Plucknett KP. Densification behaviour and microstructural evolution of Ti-48Al consolidated by spark plasma sintering. J Mater Sci 2017;52:613–27.
[26] Leon C, Rodriguez-Ortiz G, Aguilar-Reyes E. Cold compaction of metal–ceramic powders in the preparation of copper base hybrid materials. Mater Sci Eng 2009;A526:106–12.
[27] **Ceschini L, Dahle A, Gupta M, Jarfors AEW, Jayalakshmi S, Morri A, Rotundo F, Toschi S, Singh RA. Mechanical behavior of Al and Mg based nanocomposites. Aluminum and Magnesium Metal Matrix Nanocomposites. Engineering Materials. Singapore: Springer; 2017. p. 95–137**https://doi.org/10.1007/978-981-10-2681-2_4.
[28] Casati R, Vedani M. Metal matrix composites reinforced by nano-particles—a review. Metals 2014;4:65–83.
[29] Casati R, Bonollo F, Dellasega D, Fabrizi A, Timelli G, Tuissi A, Vedani M. Ex situ Al–Al 2 O 3 ultrafine grained nanocomposites produced via powder metallurgy. J Alloys Compd 2014;615:S386–8.
[30] Eldesouky A, Johnsson M, Svengren H, Attallah M, Salem H. Effect of grain size reduction of AA2124 aluminum alloy powder compacted by spark plasma sintering. J Alloys Compd 2014;609:215–21.
[31] Dieter GE, Bacon DJ. Mechanical metallurgy. New York: McGraw-Hill; 1986.
[32] Chen W-H, Lin H-T, Chen J, Nayak PK, Lee AC, Lu H-H, Huang J-L. Microstructure and wear behavior of spark plasma sintering sintered Al2O3/WC-based composite. Int J Refr Met Hard Mat 2016;54:279–83.
[33] Parrington RJ. Practical Fail Anal 2002;2:16–9.